

Femtosecond time-resolved powder diffraction experiments using hard X-ray free-electron lasers

C. Blome,^{a*} Th. Tschentscher,^a J. Davaasambu,^b P. Durand^b and S. Teichert^b

^aHASYLAB at DESY, Notkestrasse 85, D-22607 Hamburg, Germany, and ^bMax Planck Institute for Biophysical Chemistry, Am Fassberg 11, D-37070 Göttingen, Germany.

E-mail: christian.blome@desy.de

In the next decade the scientific community expects a strong impact in physics, chemistry, biology, material research and life sciences by the availability of high-brilliance X-ray radiation from free-electron laser (FEL) sources. In particular, in the field of ultrafast science these new sources will allow new types of experiments, enabling new phenomena to be discovered. Whereas today ultrafast X-ray diffraction experiments are strongly restricted by the limited X-ray flux of current sources of sub-picosecond X-ray pulses, FELs will provide short pulses of typically 10^{12} photons with a duration of the order of 100 fs and monochromaticity of 10^{-3} . Here, the feasibility of time-resolved single-shot powder diffraction experiments using these intense pulses, and the requirements of these experiments, are discussed. The detector count rates are estimated for diffraction from a model compound in a wide q -regime under the special consideration of high resolving power. In the case of LCLS radiation parameters, single-shot experiments will be feasible although high-resolution powder diffraction will require a reduction of the intrinsic FEL radiation bandwidth.

1. Introduction

Photo-induced chemical reactions and phase transitions have been observed in a time-resolved manner in the optical regime for a long period. However, optical experiments only test the electronic properties; therefore we only gain indirect information on the nuclear response. In contrast, X-rays provide the possibility of determining the geometrical structure of matter with atomic resolution. Ultrafast time-resolved X-ray diffraction has received considerable attention during recent years owing to the availability of sources of ultrashort X-ray pulses (Rousse *et al.*, 2001; Tschentscher, 2004). Experiments exhibiting temporal resolution in the sub-picosecond range investigated changes of the atomic structure on the time scale of atomic movements (Lindenberg *et al.*, 2005). The highest resolution in the determination of the three-dimensional structure of matter is obtained in single-crystal diffraction experiments. In addition, single-crystal diffraction is very efficient in that a large fraction of the incident intensity is diffracted into a single Bragg reflection. Detection of the reflected radiation is therefore facilitated. Although having a reduced resolving power and being less efficient, powder diffraction is another method for X-ray structure determination that has been shown to be versatile and powerful in many applications (Langford & Louer, 1996). Applications from the areas of material sciences and chemistry make use of the

advantage that sample preparation for powder diffraction is much simpler. There is no need to grow single crystals of considerable size and crystal quality. Furthermore, powder diffraction enables the investigation of several phases of the material at once using Rietveld refinement methods (Rietveld, 1966). With respect to the proposed experiments using free-electron laser (FEL) radiation, a further important advantage is that powder diffraction allows the entire structural information to be collected simultaneously, *i.e.* without needing to rotate or scan parts of the experimental set-up. Likewise, single-shot experiments become feasible. Despite these advantages of the powder diffraction technique, ultrafast time-resolved experiments have not been feasible up to now owing to the lack of intense ultrashort X-ray radiation sources. FEL sources for hard X-ray radiation, like the Linac Coherent Light Source (LCLS) at Stanford, USA (Arthur *et al.*, 2002), or the proposed European XFEL project in Hamburg, Germany (Brinkmann *et al.*, 2002), will provide ultrashort X-ray pulses of high enough intensity to allow this type of experiment. We therefore have proposed to carry out powder diffraction experiments yielding a time resolution of the order 100 fs using these FEL sources. In this paper we discuss the experimental requirements and the observable photon flux varying several experimental parameters.

The experiments apply the optical laser pump/X-ray probe method. Photo-excitation of the powder using ultrafast laser

light leads to a well defined initiation of the process under investigation yielding a well defined time zero. Delaying the X-ray probe with respect to the laser pump allows the time-resolved structural changes to be investigated for discrete time delays.

For the case where the probe arrives prior to the pump, the non-excited sample structure in the electronic ground state is probed. In the other case, *i.e.* pump equal or prior to probe, structural changes of the system will modify the diffraction pattern. In general, both excited as well as non-excited crystalline materials are probed. By analyzing difference maps of data sets observed for each time delay with respect to a data set obtained for an arrival of the probe (X-ray) prior to the pump (optical laser), information about the light-induced structural changes can be obtained (Davaasambuu *et al.*, 2004). The method of analyzing difference maps raises the sensitivity to the photo-induced changes of the structure since the non-excited molecules do not contribute to the difference signal. The method further allows checking for the occurrence of systematic errors like, for example, sample heating by the pump beam.

When analyzing powder diffraction patterns as a function of time, three time-dependent signal changes have to be expected: the shift of Bragg diffraction peaks, the modulation of peak intensities, including the complete occurrence/elimination of peaks owing to the change of the crystal structure, and the time-dependent changes of the peak profile owing to internal stress. The corresponding time scales range from femtoseconds to milliseconds. In general, the structural changes within the unit cell occur from femtoseconds to milliseconds and lattice relaxations from picoseconds to milliseconds. The most detailed analysis of time-resolved powder diffraction data therefore requires the application of peak profile analysis. The results to be expected from peak profile analysis depend critically on the resolution of the powder diffraction set-up. In the following we describe powder diffraction measurements for an exemplary sample system and LCLS radiation parameters, and define the requirements of the experimental set-up from this analysis.

2. The sample system

We cannot know today the exact sample material to be investigated in first experiments. Also, different samples may require varying experimental conditions. However, to make realistic estimates of diffraction patterns and detector count rates we have simulated the powder diffraction pattern for a selected sample system, methylammonium tetrachloromanganate (II) $[(\text{CH}_3\text{NH}_3)_2\text{MnCl}_4]$, hereafter MAMC. MAMC, or its related compounds, is an example of a whole class of inorganic materials undergoing structural phase transitions with large variation in electronic and magnetic properties (Adams & Stevens, 1978). Under illumination the system exhibits local as well as cooperative structural rearrangements which shall be studied using X-ray powder diffraction and other crystallographic methods.

Table 1

Parameters of the various phases of MAMC crystals.

Phases	Crystal structure	Temperature (K)
High temperature (HT)	Tetragonal	$394 < T$
Room temperature (RT)	Orthorhombic	$257 < T < 394$
Low temperature (LT)	Pseudotetragonal	$94 < T < 257$

The different phases of MAMC and the transition temperatures are summarized in Table 1. The equilibrium structures in the different phases are well characterized by neutron and X-ray diffraction (Burghardt & Gaspard, 1995; Nesbitt & Field, 1996; Rodriguez & Moreno, 1986; Morosin & Graeber, 1967). It was shown that for this class of inorganic systems phase transitions can be triggered by light (Pejakovic *et al.*, 2002). We propose to carry out experiments with the aim of investigating processes from photo-induced local disorder up to long-range ordering using the ‘optical pump/X-ray probe’ technique (Techert *et al.*, 2001; Collet *et al.*, 2003; Cavalieri *et al.*, 2005). In addition, for temperature-stabilized samples within either of the structural phases we propose to study photo-induced structural rearrangements in detail.

In Fig. 1 we have simulated the diffraction pattern of MAMC powder in its different phases. The simulations were performed using the *Powder Cell* 4.0 program (<http://www.ccp14.ac.uk/tutorial/powdcell/basic.html>) for a photon energy of $E_{\text{X-ray}} = 8.25$ keV and unpolarized radiation. They neither account for line broadening owing to the size of the illuminated sample volume nor to the grain size of the powder. Two different changes during the phase transitions are observable: the change of the peak position, and the peak intensity including complete occurrence/elimination of diffraction peaks. From Fig. 1 it can be seen that the angular range with significant scattering power extends for $E_{\text{X-ray}} = 8.25$ keV radiation up to $2\theta = 60^\circ$. Since the high-indexed reflections are more sensitive to the structural changes, we propose to cover the angular range from 0 to 60° for investigating powder samples of the class discussed here. Looking at the different phases in a certain angular range we obtain peak distances as small as 0.07° (~ 1 mrad) thus determining the requirements for angular resolution.

3. Experimental requirements

In the following we describe a proposed experimental set-up for time-resolved powder diffraction using $E_{\text{X-ray}} = 8.25$ keV FEL radiation provided by LCLS. Basic requirements for the design of an experimental set-up at LCLS will be discussed. Table 2 summarizes the LCLS FEL radiation parameters that have been used.

In Fig. 2 the proposed set-up for powder diffraction is shown. The instrumental resolution in powder diffraction experiments is determined by the X-ray beam size and divergence at the sample position, and by the X-ray energy spread. The resulting angular distribution is then sampled by the X-ray detector. In order to be able to observe small changes of diffraction peaks following laser illumination, both in position and intensity, we propose to enable powder

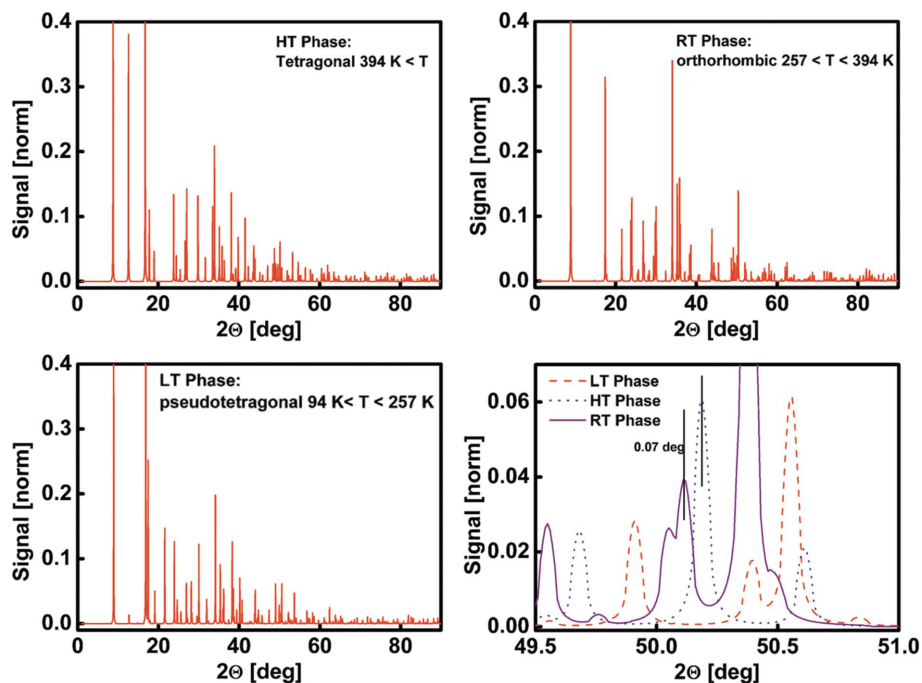


Figure 1 Radial distribution function of the powder diffraction pattern of MAMC at $E_{X\text{-ray}} = 8.25$ keV. The maximum signal is normalized to 1 for each graph. The simulation shows the variation of the diffraction pattern for the HT, RT and LT phases listed in Table 1. The lower right-hand side plot presents a magnified angular range of $2\theta = 49.5\text{--}51^\circ$.

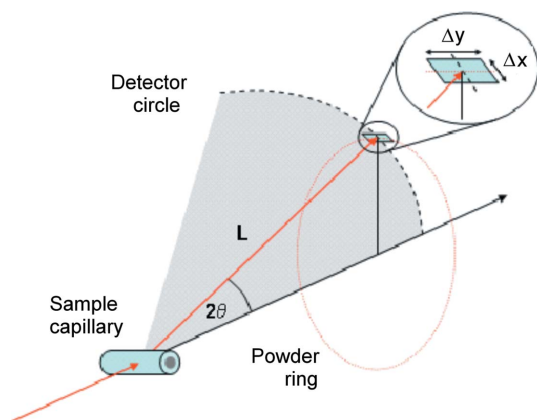


Figure 2 Sketch of the experimental set-up. For clarity only one pixel element of the line detector positioned along the broken line is shown.

Table 2

LCLS FEL radiation parameters (Arthur *et al.*, 2002) for the near and the far experimental halls. The X-ray spot sizes in the near and the far halls have been calculated in the far-field approximations for an apparent source size of $70\ \mu\text{m}$ (FWHM) and distances with respect to the end of the undulator of 120 and 390 m, respectively.

X-ray radiation properties	Unit	Near hall	Far hall
Photon energy	keV	8.27	8.27
Relative bandwidth (FWHM)	%	0.31	0.31
Pulse duration (FWHM)	fs	230	230
Repetition rate	Hz	120	120
Photons per pulse		1.9×10^{12}	1.9×10^{12}
Beam divergence (FWHM)	μrad	1	1
Beam size (FWHM)	μm	140	400

diffraction experiments with instrumental resolutions better than $500\ \mu\text{rad}$ over the entire angular range from a few degrees up to 60° . For comparison of instrumental resolution and detection systems, state-of-the-art powder diffraction instruments at synchrotron radiation sources are listed in Table 3. High-resolution set-ups until recently used analyzer crystals allowing the angular distribution to be probed with very fine resolution. High instrumental resolution, like the ones quoted in Table 3, are typically obtained at higher photon energies and will degrade when using 8.25 keV radiation. Recently, position-sensitive one-dimensional detectors have been introduced (Schmitt *et al.*, 2003) yielding reasonably high resolution.

For the LCLS FEL parameters with a very small divergence of the FEL radiation (see also Table 2) the angular resolution is determined by the angular spread $\Delta(2\theta)_{\text{geo}} = D/L$ owing to the beam size D and the sample-to-detector distance L , and by the angular spread

$\Delta(2\theta)_{\text{bw}} = 2 \tan(\theta) \Delta E/E$ owing to the radiation bandwidth. The contribution to the broadening owing to the grain size $2r$ of the powder is taken into account by the Scherrer equation, $\Delta(2\theta)_{\text{grain}} = 0.94\lambda/[2r \cos(\theta)]$, where λ is the X-ray wavelength. In Figs. 3 and 4 the total instrumental resolution $\Sigma = [\Delta(2\theta)_{\text{geo}}^2 + \Delta(2\theta)_{\text{bw}}^2 + \Delta(2\theta)_{\text{grain}}^2]^{1/2}$ is plotted as a function of scattering angle 2θ for several combinations of parameters D , L , $2r$ and $\Delta E/E$ assuming Gaussian distribution functions. Here, we use the natural FEL beam size without collimation by slits or focusing by mirrors since we would like to avoid diffraction effects that may lead to an inhomogeneous intensity distribution at the sample position. As sample-to-detector distances we assume either $L = 0.5$ or $L = 1$ m. For the bandwidth either the natural FEL bandwidth of $\Delta E/E = 0.31\%$ or the usual monochromator bandwidth of $\Delta E/E \simeq 0.01\%$ applying diamond crystals are used.

According to Fig. 3(a) the contribution of the bandwidth is dominant for the non-monochromatic FEL beam resulting in an instrumental resolution of the order of a few mrad. In Fig. 3(b) the broadening is shown for typical sizes of D , L and $2r$ and a bandwidth of 10^{-4} . In this situation the total instrumental resolution is dominated by the grain size and the geometrical contribution. A total instrumental resolution of the order of 1 mrad can be achieved over the entire angular range. Fig. 4 shows the total instrumental resolution for a powder with $2r = 1\ \mu\text{m}$ particle size and various settings of D , L and $\Delta E/E$. The contribution owing to grain size can be neglected in this case. In Fig. 4(a) the given natural bandwidth is assumed and broadening again is dominated by the bandwidth contribution.

Table 3

Instrumental resolution and detection systems of synchrotron radiation-based powder diffraction beamlines.

Facility (beamline)	Detection system	Resolution (μrad)	Reference
ESRF (ID31)	Nine-crystal analyzer stage	52.4	Fitch (2004)
NLSL (X3B1)	One-crystal analyzer stage	350	Ha <i>et al.</i> (1999)
SLS (MS)	Five-crystal analyser stage	35	Gozzo <i>et al.</i> (2004)
	One-dimensional microstrip detector	210	Gozzo <i>et al.</i> (2004)

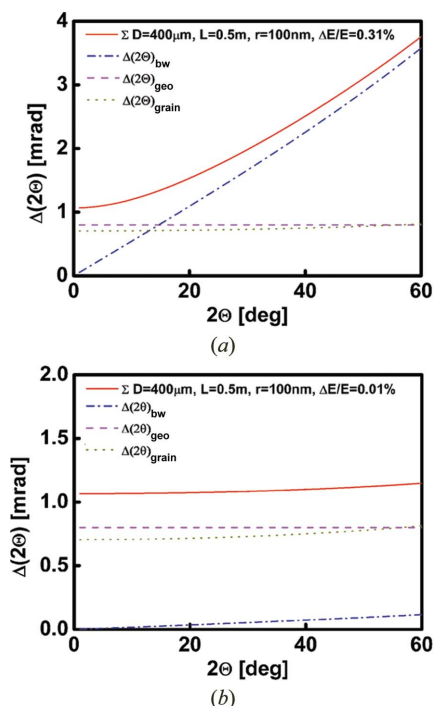


Figure 3

Instrumental resolution as a function of scattering angle 2θ in the case of a powder with a grain size of $2r = 200\text{nm}$. The plots present the total instrumental resolution Σ with their contributions owing to geometry $\Delta(2\theta)_{geo}$, bandwidth $\Delta(2\theta)_{bw}$ and grain size $\Delta(2\theta)_{grain}$. The parameter set corresponds to the beam size in the far hall and $L = 0.5\text{m}$. In (a) the natural bandwidth of the FEL was assumed. In (b) a bandwidth of $\Delta E/E = 10^{-4}$ was applied to take into account the bandwidth of a monochromator.

In Fig. 4(b) a monochromator is taken into account and the angular resolution is determined by the geometrical contribution D/L . By using micrometre-grained powder and a small bandwidth a resolution of $300\mu\text{rad}$ is best achievable. This situation can be further improved by applying focusing X-ray optics to decrease the ratio D/L .

3.1. Detector requirements

We propose to sample the resulting angular profile by direct detection of the diffracted X-ray beam with a spatially resolving detector. Compared with a crystal analyzer the direct detection method has higher throughput and avoids scanning procedures, thus allowing for single-shot data collection.

Table 4

Parameters for a linear detector covering 2θ angles from 0 to 60° . The instrumental resolutions Σ are derived from Fig. 4, assuming a bandwidth of 10^{-4} and a micrometre-grained powder.

Location	L (m)	Σ (μrad)	Δx (μm)	$\Delta(2\theta)_{\text{pixel}}$ (μrad)	Pixels
Near hall	0.5	350	20	40	13000
Near hall	1.0	250	20	20	26000
Far hall	1.0	450	50	50	10000

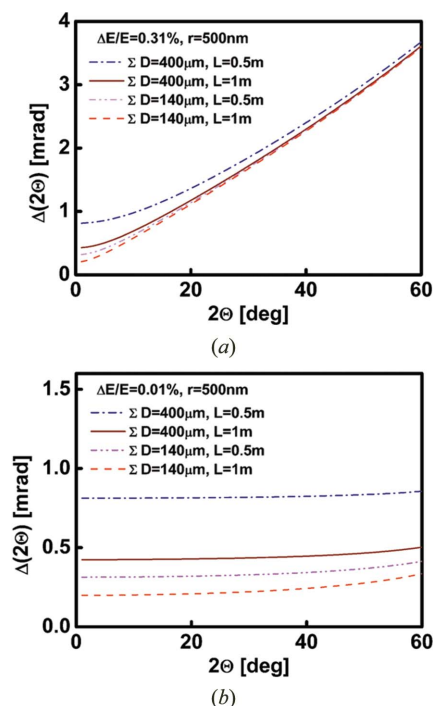


Figure 4

Instrumental resolution as a function of scattering angle 2θ in the case of a powder with a grain size of $2r = 1\mu\text{m}$. Both plots show the total instrumental resolution Σ for various sets of parameters. In (a) the natural FEL bandwidth is shown and for (b) a monochromatic beam was taken into consideration.

Owing to the statistical fluctuations and the moderate repetition rate of 120Hz we propose to use a detector covering the entire angular range from 0 to 60° simultaneously. To cover this large range the detector elements need to be positioned on a sphere around the sample position. For mechanical reasons, and since the observable count rate is high enough, the limitation to a line detector, positioned on a circle segment around the sample position, will be sufficient. The spatial resolution of the detector Δx relating to the angular broadening Σ must be such that peak profile analysis procedures can be applied. Ideally the pixel pitch should be of the order of $0.1L\Sigma$.

The above-addressed requirements lead us to suggest the use of a one-dimensional or microstrip detector with high spatial resolution in one coordinate. Table 4 provides three sets of typical detector parameters corresponding to the above-discussed quantities. The pixel sizes and detector distances had been chosen to reach angular resolutions of $\Delta(2\theta)_{\text{pixel}}$, which are adequate to sample the angular instru-

mental resolution. A full coverage in 2θ is assumed, which corresponds to a very small dead area between pixels. Owing to the linear polarization of the FEL beam the detector should operate in the vertical plane. The width of the pixels could be several mm in order to integrate intensity along the powder ring. The resulting broadening of the angular resolution can be neglected for scattering angles 2θ larger than 10° . A detector with very close geometrical parameters was recently applied in high-resolution powder diffraction experiments (Schmitt *et al.*, 2003; Gozzo *et al.*, 2004).

Other detector requirements concern the signal detection. The detector shall allow for 120 Hz readout with a low noise. In order to collect the signal from many X-ray photons arriving at the detector within a single exposure, the electronic signal must be integrating. However, in order to be able to detect small diffraction peaks and also small changes in the intensity, single-photon sensitivity will be required, *i.e.* the noise level is significantly smaller than the signal which corresponds to one X-ray photon. As follows from the estimation of count rates in §4, a resolution of at least 12 bit (up to 4000 photons per pixel) will be required.

3.2. Other experimental requirements

We expect a penetration depth of the optical excitation laser for MAMC samples of, at maximum, 50 μm within the entire spectral range (for general considerations, see Morosin & Graeber, 1967). To avoid spatial mismatch of the penetration of the optical and X-ray radiation, and thereby to maximize the observable signal, the sample thickness should be of the order of the penetration depth of the optical radiation. The issue of the optimal excitation and spatial overlap of the optical light pump and X-ray probe beams has very intensively been discussed by Davaasambuu *et al.* (2004). In the following we assume 100 μm -thick samples. For rotation-symmetric samples one thus pre-determines one transverse dimension. It follows that an optical and X-ray beam size of the order of 100 μm will make best use of the provided X-ray flux.

In the following we describe sample preparation techniques allowing the preparation of samples with thicknesses from 10 to 100 μm . Recent time-resolved X-ray diffraction experiments on MAMC derivatives suggest upon photo-excitation that X-ray diffraction signal changes of the order of $\Delta I/I = 10\%$ can be expected for the ultrafast time scale (Durand & Techert, 2005). Two sample preparation methods are proposed that have been tested using optical laser excitation and synchrotron radiation-based X-ray beam with good experience. The standard method for powder diffraction is to use thin capillaries filled with powder. Capillaries are available with an inner diameter of $>5 \mu\text{m}$ and can therefore be used even for the thinnest samples. This method has the advantage of well defined and uniform sample geometry and absorption lengths. For convenience we use this sample geometry in §4 to estimate observable count rates. A problem for capillaries is the X-ray scattering from the capillary walls with typical thicknesses of 50–100 μm . Since the capillaries are made of borosilicate, aluminosilicate or quartz the resulting amor-

phous scattering pattern will lead to a high background in the powder diffraction signal. To overcome this problem, an alternative sample preparation method using thin films can be applied (Davaasambuu *et al.*, 2004). The thickness and the flatness of the sample are checked by interferometric methods and by measuring the optical density of the material knowing the extinction coefficient. Again, the powder diffraction signal is superimposed by the amorphous scattering from the coating cover. Both preparation methods are suitable, but owing to absorption in the glass capillary and higher background by strong scattering of the capillary the second method has higher potential. To further improve the signal-to-background ratio, new techniques, including the preparation of powder samples with thicknesses smaller than 10 μm or thin single crystals, have to be developed.

For powder diffraction of samples of thicknesses described above the question of preferred orientation needs to be addressed. We believe that our experimental approach of looking at differences of data sets with laser excitation before (positive time point) and after (negative time point) the X-ray probe allows the problem of preferred orientation to be avoided. We assume here that single grains do not move during the single-shot exposures, which is very unlikely. It is required, however, to store data for single-shot exposures together with the corresponding information of relevant experimental parameters, *e.g.* the timing of the optical laser with respect to the X-ray pulse.

To characterize the damage owing to X-ray exposure we have calculated the amount of energy that is deposited in the sample volume. For the experimental parameters proposed below (see Table 5, bandwidth is limited by a monochromator), $\sim 9 \times 10^9$ photons are absorbed inside the sample, corresponding to $\sim 12 \mu\text{J}$ energy deposition per pulse. For the solid-state density of 1.7 g cm^{-3} and a sample volume of $\pi \times 140 \times 25^2 \mu\text{m}^3$ a specific energy deposition of 25 J g^{-1} follows. This value corresponds to an absorbed energy of 50 meV per molecule and pulse. The corresponding temperature increase is estimated from $\Delta T = E/(mc_p)$ where E is the deposited energy in the sample volume, m is the mass of the sample volume in mol, and c_p is the heat capacity in $\text{J mol}^{-1} \text{ K}^{-1}$. Since the value of c_p for MAMC is not available, we used the value for the similar compound MaFeC, $\sim 240 \text{ J mol}^{-1} \text{ K}^{-1}$, for the temperature range 240–350 K (Goto *et al.*, 1982). We estimate a temperature increase of 10 K per pulse for an energy absorption of 50 meV per molecule and pulse. Using cryogenic cooling of the relatively small samples we estimate that heat conduction is high enough to compensate for the temperature steps for the 120 Hz repetition rate of the X-ray pulses. Since the X-ray scattering itself occurs on time scales much shorter than the thermodynamical heating of the sample, it is assumed that for this case the investigation of the sample structure is not severely affected by the energy deposition. For longer exposure times the energy absorption certainly leads to radiation-induced degradation of the samples. This radiation damage has been investigated intensively for proteins (Burmeister, 2000; Weik *et al.*, 2000, 2002).

Table 5

Parameters used for the evaluation of single-shot detector count rates.

Parameter	Unit	Value
No. of photons, N_{eff}		4.27×10^9
X-ray energy, $E_{\text{X-ray}}$	keV	8.25
X-ray bandwidth		10^{-4}
Polarization		100% linear
Beam size, D	μm	140
Sample thickness	μm	50
Capillary wall thickness	μm	50
Sample-to-detector, L	mm	500
Pixel size, $\Delta x \times \Delta y$	$\mu\text{m} \times \mu\text{m}$	20×1000
Detection efficiency		100%

In the case of using the natural FEL bandwidth and otherwise identical experimental conditions the X-ray flux increases by a factor of 50 leading to an absorbed energy of 2.2 eV per molecule. This value corresponds to a temperature increase of 500 K per X-ray pulse. Since such temperature variation certainly alters the sample structure, it is proposed to use sample changing schemes for pulse-to-pulse exchange at a repetition rate of 120 Hz. To investigate the structural changes owing to X-ray energy deposition of the order of magnitude calculated above, illuminating samples with comparable doses using focused pink beam at synchrotron radiation facilities is suggested.

The minimization of damage owing to the optical excitation pulse requires special attention and individual experimental investigation for every system. Experimental parameters like pulse duration, wavelength, repetition rate and power will have to be optimized for the specific sample material, *i.e.* MAMC has a strong absorption band in the regime of 430 nm. To overcome the issues of X-ray radiation damage the sample holder must foresee the continuous, or at least fast, exchange of the sample volume under investigation. For capillaries, a simple translation may be used; for flat samples, a rotating sample stage will allow continuous volume exchange. In addition, it should be foreseen to mount several samples simultaneously in a cartridge allowing easy exchange.

For the optical pump we propose to use a Ti:Sa femtosecond laser system with a pulse duration of the order of $\tau = 100$ fs with the possibility of providing stretched pulses with duration up to 10 ps. The wavelength should be continuously tunable from $\lambda = 266$ nm to $\lambda = 1500$ nm. The number of photons per pulse delivered at the sample position should be of the order 10^{15} in the focal spot for all wavelengths. This number (~ 1 mJ laser energy at 400 nm per pulse) corresponds to the number of optically excited molecules in the probed sample volume. An optical laser beam with focal spot diameter of 100 μm will be required for the experiments. To avoid smearing of the temporal resolution the laser should impinge the sample in a collinear optical pump/X-ray probe geometry.

The experiments will require diagnostic tools for the FEL beam. The incoming intensity as well as the photon energy spectrum needs to be collected, in general on a pulse-to-pulse basis. The arrival time of the FEL pulse relative to the optical laser pulse needs to be determined. This task could be achieved using electro-optical sampling techniques (Cavalieri

Table 6

Transmission coefficients used for the evaluation of usable X-ray flux.

Material	Path	Coefficient at 8.25 keV
Air	50 cm	0.9795
SiO ₂	100 μm	0.43
Sample	50 μm	0.41

et al., 2005). To collect data of various diagnostic systems the data acquisition must allow synchronization of the signals and data sets at the frequency of the experiment, up to 120 Hz.

4. Intensity distribution in physical units

In this section we estimate the intensity in a detector pixel assuming the experimental parameters derived above and listed in Table 5. In doing this, we assume 100% photo-transformation of the material which is evidently an over-estimation. However, photo-transformations of the order of 20–50% are realistic (Collet *et al.*, 2003; Davaasambuu *et al.*, 2005). For improving the visualization of photo-transformed materials the procedure of taking difference maps with 100% photo-excitation has been developed (Schotte *et al.*, 2004).

Let us first consider the absorption of X-rays owing to scattering in the sample and its environment. For this purpose we factorize the absorption owing to the capillary walls (two times), an air path of $L = 500$ mm from the sample to the detector, and absorption by a 50 μm -thick MAMC powder. Table 6 summarizes the calculated transmission coefficients (see http://www-cxro.lbl.gov/optical_constants).

The glass capillary forms a hard aperture for an X-ray beam with Gaussian intensity distribution in both lateral dimensions resulting in a transmission factor of $T_{\text{geo}} = 0.33$. The restricted bandwidth of the monochromator gives an additional loss of $T_{\text{bw}} = 0.023$. For the total transmission T , $T = T_{\text{sample}} T_{\text{SiO}_2} T_{\text{air}} T_{\text{geo}} T_{\text{bw}} = 0.0013$. Therefore the number of detectable photons is $N_{\text{eff}} = 2 \times 10^{12} T$.

For a cylindrical specimen illuminated by a linearly polarized beam, the integrated number of photons N_{hkl} of a segment of length Δy (see Fig. 2) for a Bragg reflection from hkl planes recorded at a distance L is

$$N_{hkl} = \frac{N_{\text{eff}}}{A} \left(\frac{e^4}{m_e^2 c^4} \right) \frac{V \lambda^3 m |F_{hkl}|^2}{4v^2} \frac{1}{\sin(\Theta)} \frac{\Delta y}{2\pi L \sin(2\Theta)}. \quad (1)$$

Here, A is the effective area formed by the hard aperture of the capillary, V is the sample volume, v is the unit-cell volume and m is the multiplicity. The other terms have their usual significance for scattering experiments (Warren, 1990). The derived formula is valid for the described detector geometry, *i.e.* the FEL beam is polarized horizontally and the detector operates in the vertical plane. Fig. 5 shows the integrated photon flux as a function of 2Θ .

In the angular regime of 50–60° we calculate an integrated X-ray intensity of $N_{hkl} = 20$ –80 photons per reflection hkl and recorded pulse. The X-ray intensity increases linearly with the transversal pixel size Δy . Since it is possible to increase the

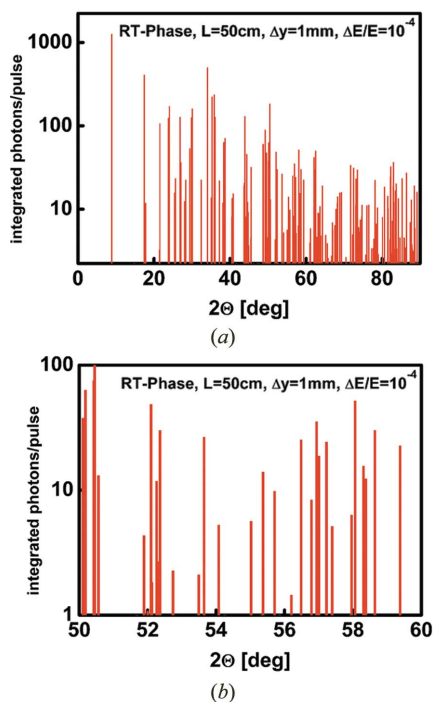


Figure 5 Detector count rates for the entire angular range (a) and the high- 2θ region (b). The plots indicate the number of integrated photons N_{hkl} per X-ray pulse for the parameters given in Table 5 including absorption.

size to 10 mm without losing the angular resolution, one could achieve integrated intensities of 200–800 photons per pulse. To observe a statistical accuracy around 1% would require collecting of the order of 10–50 pulses. It should be noted that these data have also to be analysed and binned in terms of fluctuations of the experimental parameters (*e.g.* the time delay, photon energy, beam position). In general, it will therefore be required to collect at least one order of magnitude more pulses to achieve the required statistical accuracy.

In the long term, one possibility for increasing the integrated intensities is to increase the peak brilliance by self-seeding the FEL process leading to a smaller bandwidth (Feldhaus *et al.*, 1997). In this situation the complete intensity will be in a narrow spectral bandwidth and the losses by a monochromator can be avoided. An intensity increase of $\sim 1/T_{bw} = 40$ would lead to integrated intensities of 8000–32000 photons per shot for the above-discussed configuration. These intensities are likely to provide significant statistical accuracy for single-shot exposures. Another idea to increase the intensity for the first experiments at LCLS is removing the monochromator and to operate at lower resolution. Again, intensities such as those for a self-seeded FEL could be obtained and will satisfy the required statistical accuracy.

To discuss the possibility of line-fitting procedures we need to calculate the diffracted photons per pixel N_p . We therefore normalize N_{hkl} to the width of the Bragg peak Σ , resulting in the averaged number of photons per radian, and multiply by the angular size of the pixel, $\Delta(2\Theta)_{\text{pixel}}$,

$$N_p = N_{hkl} \Delta(2\Theta)_{\text{pixel}} / \Sigma. \quad (2)$$

For the parameters discussed in this section one obtains an almost constant line broadening of $\Sigma = 0.2$ mrad over the entire range of diffraction angles (parameter set not shown in Fig. 3: $D = 50 \mu\text{m}$, $L = 0.5$ m, $\Delta E/E = 10^{-4}$, $r = 500$ nm, $\Delta x = 20 \mu\text{m}$). With $\Delta(2\Theta)_{\text{pixel}} = \Delta x/L$ we calculate a constant factor for $\Delta(2\Theta)_{\text{pixel}}/\Sigma$ of 0.2. Taking Fig. 5, one thus estimates, for the angular regime of 50–60°, about 4–16 photons per shot in a pixel of the size $20 \mu\text{m} \times 1000 \mu\text{m}$, or 40–160 per shot for a $20 \mu\text{m} \times 10000 \mu\text{m}$ pixel. If the powder lines are broadened owing to grain size or strain effects, the intensity per pixel will decrease. Such intensities are likely to miss statistical significance allowing line-fitting procedures for single pulse experiments. From experience with laser plasma-based experiments we estimate a statistical relevant intensity of about 2000 photons per pixel (Blome, 2003). For experiments using the natural bandwidth of FEL radiation resulting in higher X-ray intensity the instrumental resolution will be dominated by the bandwidth of the source (compare Fig. 3) and results in a broadening of a few mrad independently of the grain size. For simplicity we assume a constant broadening of $\Sigma = 3$ mrad over the entire range of diffraction angles. For $L = 0.5$ m and $\Delta x = 20 \mu\text{m}$ it follows that $\Delta(2\Theta)_{\text{pixel}}/\Sigma = 0.014$, resulting in an X-ray intensity of roughly 100–450 photons per pulse and per $20 \mu\text{m} \times 10000 \mu\text{m}$ pixel. Since the instrumental resolution is largely over-sampled using the $20 \mu\text{m}$ pixels one can apply software binning to increase the physical pixel size and therefore the number of photons per pixel. By applying suitable X-ray optics the geometrical transmission factor can be raised by a factor of three.

The coherent illumination using FEL radiation will lead to interference effects in the diffraction pattern. The average size δ of the produced speckles scales with the inverse of the illuminated region $1/D$, the wavelength λ and the distance between sample and detector L : $\delta = 2\lambda L/D$ (Svelto, 1976). For an illuminated region of $140 \mu\text{m}$, a wavelength corresponding to 8.25 keV and a distance of $L = 0.5$ m, one estimates an averaged angular speckle size of 1.5 μrad . Since the achievable angular resolution is in the regime of a few 100 μrad , the proposed instrument will not resolve individual speckles and the coherent illumination should not affect the observable diffraction pattern.

Finally, we have to discuss the background signal overlaying the diffraction signal at the detector. Background can arise owing to scattering from the environment (*e.g.* radiation background in the experimental area, scattering halo around the X-ray beam impinging on the sample), scattering from air, scattering from the sample container, and electronic noise in the integrating detector. In general, the beam path in air needs to be reduced to a minimum by using either evacuated or helium-filled tubes or inert gas environments. Scattering from the glass capillaries is a serious source of background that cannot be avoided, *e.g.* by using collimation schemes, owing to its small distance to the sample volume. Here the development of better sample containers, like those discussed in the sample preparation section above, will improve the situation largely.

Finally, for the detection, single-photon sensitivity is requested providing the possibility of suppressing electronic noise in the detection scheme.

5. Conclusions

We propose to carry out time-resolved powder diffraction experiments using 0.15 nm FEL radiation provided by LCLS. The experiments aim to follow structural changes of photo-induced phase transitions and photo-induced structural distortions in solid organic and inorganic materials. Powder samples will be prepared with thicknesses of less than 100 μm in order to maximize the signal-to-noise ratio. Simulations for a relevant powder sample indicate that, for the LCLS photon energy, the angular range up to 60° can be investigated, improving the accuracy of the structure determination. To allow peak profile analysis the experiments require high instrumental resolution. Analysis of the instrumental resolution shows that it is required to monochromatize the FEL radiation in order to obtain high-resolution conditions. The beam size at the sample position should be of the order of 100 μm to obtain high-flux experiments; therefore the experiments need either to be carried out in the near experimental hall or use focusing of the radiation.

By using a monochromatic X-ray beam, the energy deposition in the sample volume will lead to temperature steps of the order of 10 K. Using cryo-cooling this temperature oscillation is not expected to cause severe problems. For larger X-ray fluences, *e.g.* for pink or seeded FEL beams, sample exchange systems will need to be applied. We propose to use a one-dimensional linear array of pixel detectors with a size of 20–50 μm \times 10000 μm , fully covering the scattering angle 2θ from 0 to 60° in a curved vertical scattering geometry. Calculations of the expected detector count rates have been carried out for a model compound in a relevant angular range. They show that, in the case of a typical monochromator bandwidth, a pixel size of 20 μm \times 10000 μm X-ray intensities per pulse and pixel vary from 40 to 160 photons in the angular regime of 50–60°. Without monochromator, a count rate per pulse and pixel of 100–450 photons will be achieved at the expense of lowering the instrumental resolution. Since sample damage can be neglected, a repetition rate of 120 Hz with the monochromatic full X-ray beam can be accepted.

The authors gratefully acknowledge Ivan Vartanians for discussions concerning the coherence effects.

References

- Adams, D. M. & Stevens, D. C. (1978). *J. Phys. C*, **11**, 617–632.
- Arthur, J. *et al.* (2002). SLAC-R-593, SLAC, Menlo Park, CA, USA.
- Blome, C. (2003). PhD thesis, University of Essen, Germany.
- Brinkmann, R. *et al.* (2002). TESLA XFEL Technical Design Report, DESY 2002–167. DESY, Hamburg, Germany.
- Burghardt, I. & Gaspard, P. (1995). *J. Phys. Chem.* **99**, 2732–2752.
- Burmeister, W. (2000). *Acta Cryst.* **D56**, 328–341.
- Cavalieri, A., Fritz, D. M., Lee, S. H., Bucksbaum, P. H., Reis, D. A., Rudati, J., Mills, D. M., Fuoss, P. H., Stephenson, G. B., Kao, C. C., Siddons, D. P., Lowney, D. P., MacPhee, A. G., Weinstein, D., Falcone, R. W. *et al.* (2005). *Phys. Rev. Lett.* **94**, 114801.
- Collet, E., Lemée-Cailleau, M.-H., Buron-Le Cointe, M., Cailleau, H., Wulff, M., Luty, T., Koshihara, S.-Y., Meyer, M., Toupet, L., Rabiller, P. & Techert, S. (2003). *Science*, **300**, 612–615.
- Davaasambuu, J., Durand, P. & Techert, S. (2004). *J. Synchrotron Rad.* **11**, 483–489.
- Durand, P. & Techert, S. (2005). Submitted.
- Feldhaus, J., Saldin, E. L., Schneider, J. R., Schneidmiller, E. A. & Yurkov, M. V. (1997). *Opt. Commun.* **140**, 341–352.
- Fitch, A. N. (2004). *J. Res. NIST*, **109**, 133–142.
- Goto, T., Yoshizawa, M., Tamaki, A. & Fujimura, T. (1982). *J. Phys. C*, **15**, 3041–3052.
- Gozzo, F., Schmitt, B., Bortolamedi, Th., Giannini, C., Guagliardi, A., Lange, M., Meister, D., Maden, D., Willmott, P. & Patterson, B. D. (2004). *J. Alloy. Comp.* **362**, 206–217.
- Ha, C., Ciria, M., O’Handley, R. C., Stephens, P. W. & Pagola, S. (1999). *Phys. Rev. B*, **60**, 13780–13785.
- Langford, I. & Louer, D. (1996). *Rep. Prog. Phys.* **59**, 131–234.
- Lindenberg, A., Larsson, J., Sokolowski-Tinten, K., Gaffney, K. J., Blome, C., Synnergren, O., Sheppard, J., Coleman, C., MacPhee, A. G., Weinstein, D., Lowney, D. P., Allison, T. K., Matthews, T., Falcone, R. W. & Cavalieri, A. L. (2005). *Science*, **308**, 392–395.
- Morosin, B. & Graeber, E. J. (1967). *Acta Cryst.* **23**, 766–770.
- Nesbitt, S. & Field, R. (1996). *J. Phys. Chem.* **100**, 12735–12756.
- Pejakovic, D. A., Kitamura, C., Miller, J. S. & Epstein, A. J. (2002). *Phys. Rev. Lett.* **88**, 057202.
- Rietveld, H. M. (1966). *Acta Cryst.* **20**, 508–513.
- Rodriguez, F. & Moreno, R. (1986). *J. Chem. Phys.* **84**, 692–697.
- Rousse, A., Rischel, C. & Gauthier, J.-C. (2001). *Rev. Mod. Phys.* **73**, 17–31.
- Schmitt, B., Brönnimann, Ch., Eikenberry, E. F., Gozzo, F., Hörmann, C., Horisberger, R. & Patterson, B. (2003). *Nucl. Instrum. Methods*, **A501**, 267–272.
- Schotte, F., Soman, J., Olson, J. S., Wulff, M. & Anfinrud, P. A. (2004). *J. Struct. Biol.* **147**, 235–246.
- Svelto, O. (1976). *Principles of Lasers*. New York: Plenum.
- Techert, S., Schotte, F. & Wulff, M. (2001). *Phys. Rev. Lett.* **86**, 2030–2033.
- Tschentscher, Th. (2004). *Chem. Phys.* **299**, 271–276.
- Warren, B. E. (1990). *X-ray Diffraction*. New York: Dover.
- Weik, M., Berges, J., Raves, M. L., Gros, P., McSweeney, S., Silman, I., Sussman, J. L., Houee-Levin, C. & Ravelli, R. B. G. (2002). *J. Synchrotron Rad.* **9**, 342–346.
- Weik, M., Ravelli, R. B., Kryger, G., McSweeney, S., Raves, M. L., Harel, M., Gros, P., Silman, I., Kroon, J. & Sussman, J. L. (2000). *Proc. Natl. Acad. Sci. USA*, **97**, 623–628.